Beta Beams

Mauro Mezzetto

INFN - Sezione di Padova

Key Words kw1, kw2, kw3

Abstract

CONTENTS

1 Neutrino Oscillations

The observation of neutrino oscillations has now established beyond doubt that neutrinos have mass and mix. This existence of neutrino masses is in fact the first solid experimental fact requiring physics beyond the Standard Model.

Neutrino oscillations are consistently described by three families ν_1, ν_2, ν_3 with mass values m_1, m_2 and m_3 that are connected to the flavor eigenstates ν_e, $\nu_\mu$and ν_τ by a mixing matrix U. The neutrino oscillation probability depends on three mixing angles, $\theta_{12}, \theta_{23}, \theta_{13}$, two mass differences, $\Delta m^2_{12} = m^2_2 - m^2_1$, $\Delta m^2_{23} = m^2_3 - m^2_2$, and a CP phase $\delta_{\rm CP}$. Additional phases are present in case neutrinos are Majorana particles, but they do not influence neutrino flavor oscillations at all.

The best-fit values and allowed range of values of the oscillation parameters at different CL, as obtained in (1), are shown in Table 1.

1.1 Future Discoveries in Neutrino Oscillations

Three parameters have not yet been measured in neutrino oscillations: θ_{13}, sign(Δm^2_{23}) and $\delta_{\rm CP}$.

The mixing angle θ_{13} is the key parameter of three-neutrino oscillations and regulates at the first order all the oscillation processes that could contribute to the measurement of sign(Δm^2_{23}) and $\delta_{\rm CP}$.

The neutrino mass hierarchy, the order by which mass eigenstates are coupled to flavor eigenstates, can be fixed by measuring the sign of Δm^2_{23}. Its value could

be +1 (normal hierarchy), in which case ν_e would be the lightest neutrino, or -1 (inverted hierarchy), for which ν_e would be the heaviest. Its value is of great importance for double-beta decay experiments (2) and for grand unification model building.

The CP phase $\delta_{\rm CP}$ is the holy grail of ultimate neutrino oscillation searches. The demonstration of CP violation in the lepton sector (LCPV) and the knowledge of the value of this phase would be crucial to understanding the origin of the baryon asymmetry in the universe, providing a strong indication, though not proof, that leptogenesis is the explanation for the observed baryon asymmetry of the Universe (3).

All these parameters can be measured via subleading $\nu_\mu \rightarrow \nu_e$ oscillations that represent the key process of any future new discovery in neutrino oscillation physics.

1.1.1 How to measure leptonic CP violation The phenomenon of CP (or T) violation in neutrino oscillations manifests itself by a difference in the oscillation probabilities of say, $P(\nu_\mu \rightarrow \nu_e)$ vs $P(\overline{\nu}_\mu \rightarrow \overline{\nu}_e)$ (CP violation), or $P(\nu_\mu \rightarrow \nu_e)$ vs $P(\nu_e \rightarrow \nu_\mu)$ (T violation).

Extensive studies, such as those published in a CERN yellow report (4), the European Network BENE (5) or the International Scoping Study (6) have been already perfomed to establish the physics potential of future facilities in discovering leptonic CP violation.

When matter effects are not negligible, following Eq. (1) of (7), the transition probability $\nu_e \rightarrow \nu_\mu$ ($\bar{\nu}_e \rightarrow \bar{\nu}_\mu$) at second order in perturbation theory in θ_{13},

$\Delta m^2_{12}/\Delta m^2_{23}$, $|\Delta m^2_{12}/a|$ and $\Delta m^2_{12}L/E_\nu$ is:

$$P^{\pm}(\nu_e \to \nu_\mu) = X_\pm \sin^2(2\theta_{13}) + Y_\pm \cos(\theta_{13})\sin(2\theta_{13})\cos\left(\pm\delta - \frac{\Delta m^2_{23}L}{4E_\nu}\right) + Z\,, \tag{1}$$

where $\pm$ refers to neutrinos and antineutrinos, respectively. The coefficients of the two equations are:

$$\begin{cases} X_\pm &= \sin^2(\theta_{23})\left(\frac{\Delta m^2_{23}}{|a-\Delta m^2_{23}|}\right)^2 \sin^2\left(\frac{|a-\Delta m^2_{23}|L}{4E_\nu}\right)\,, \\ Y_\pm &= \sin(2\theta_{12})\sin(2\theta_{23})\left(\frac{\Delta m^2_{12}}{a}\right)\left(\frac{\Delta m^2_{23}}{|a-\Delta m^2_{23}|}\right)\sin\left(\frac{aL}{4E_\nu}\right)\sin\left(\frac{|a-\Delta m^2_{23}|L}{4E_\nu}\right)\,, \\ Z &= \cos^2(\theta_{23})\sin^2(2\theta_{12})\left(\frac{\Delta m^2_{12}}{a}\right)^2\sin^2\left(\frac{aL}{4E_\nu}\right) \end{cases} \tag{2}$$

$a[\mathrm{eV}^2] = \pm 2\sqrt{2}G_F n_e E_\nu = 7.6{\cdot}10^{-5}\rho[g/cm^3]E_\nu[\mathrm{GeV}]$. changes sign by changing neutrinos with antineutrinos.

θ_{13} searches look for experimental evidence of ν_e appearance in excess of what is expected from the solar terms. These measurements will be experimentally hard because the present limit on θ_{13} , $\sin^2\theta_{13} \leq 0.035$ (0.056), 90%CL (3σ) (1) , translates into a $\nu_\mu \to \nu_e$ appearance probability much smaller than 10% at the appearance maximum in a high energy muon neutrino beam.

One of the interesting aspects of Eq. (1) is the occurrence of matter effects which, unlike the straightforward θ_{13} term, depends on the sign of the mass difference sign(Δm^2_{23}). These terms should allow extraction of the mass hierarchy, but could also be seen as a background to the CP violating effect, from which they can be distinguished by the very different neutrino energy dependence.

The CP violation can be seen as interference between the solar and atmospheric

oscillation for the same transition. Of experimental interest is the CP-violating asymmetry A_{CP}:

$$A_{CP} = \frac{P(\nu_\mu \to \nu_e) - P(\overline{\nu}_\mu \to \overline{\nu}_e)}{P(\nu_\mu \to \nu_e) + P(\overline{\nu}_\mu \to \overline{\nu}_e)} \tag{3}$$

displayed in Fig. 1, or the equivalent time reversal asymmetry A_T.

1.1.2 The problem of degenerate solutions The richness of the $\nu_\mu \to \nu_e$ transition is also its weakness: it will be very difficult for pioneering experiments to extract all the genuine parameters unambiguously. Due to the three-flavor structure of the oscillation probabilities, for a given experimental result several different disconnected regions of the multi-dimensional space of parameters could fit the experimental data, originating degenerate solutions.

Traditionally these degeneracies are referred as The intrinsic or $(\delta_{\rm CP}, \theta_{13})$-degeneracy (7); the hierarchy or sign(Δm^2_{31})-degeneracy (8); the octant or θ_{23}-degeneracy (9). This leads to an eight-fold ambiguity in θ_{13} and $\delta_{\rm CP}$ (10), and hence degeneracies provide a serious limitation for the determination of θ_{13}, $\delta_{\rm CP}$, and the sign of Δm^2_{31}.

1.2 Experimental Setups

1.2.1 Conventional neutrino beams Conventional neutrino beams are produced through the decay of π and K mesons generated by a high energy proton beam hitting small Z, needle-shaped, segmented targets. Positive (negative) mesons are sign-selected and focused (defocused) by large acceptance magnetic lenses into a long evacuated decay tunnel where ν_μ's ($\overline{\nu}_\mu$'s) are generated.

In case of positive charge selection, the ν_μ beam has typically a few percent of $\overline{\nu}_\mu$ contamination (from the decay of the residual π^-, K^- and K^0) and $\sim 1\%$ of ν_e and $\overline{\nu}_e$ coming from three-body $K^\pm$, K_0 decays and μ decays.

The precision of the evaluation of the intrinsic ν_e to ν_μ contamination is limited by the knowledge of the π and K production in the primary proton beam target requiring a devoted hadroproduction experiment like the Harp experiment (11) that measured both the K2K (12) and the MiniBooNE (13) targets, covering most of the useful pion phase-space, successfully improving the description of the two beam lines.

Close detectors are used to directly measure beam neutrinos and backgrounds (for a discussion about close detectors in future LBL experiments see (14)).

Current long-baseline experiments with conventional neutrino beams can look for $\nu_\mu \rightarrow \nu_e$ transitions even if they are not optimized for such studies.

The K2K experiment published an analysis about ν_e appearance (16), still not improving the Chooz limit.

MINOS at NuMI (17) has already published preliminary results (18) showing a statistically not significative excess of ν_e-like events in the data sample.

The OPERA detector (19) at the CNGS (20) is also suited for electron detection, it can reach a 90% CL sensitivity of $\sin^2 2\theta_{13} = 0.06$ ($\Delta m^2_{23} = 2.5{\cdot}10^{-3}$ eV^2), (21), for five years exposure to the CNGS beam at nominal intensity of $4.5{\cdot}10^{19}$ pot/yr.

1.2.2 Second generation long-baseline experiments The focus of second generation LBL experiments will be the measurement of θ_{13} through the detection of sub-leading $\nu_\mu \rightarrow \nu_e$ oscillations.

According to the present experimental situation, conventional neutrino beams can be improved and optimized for the $\nu_\mu \rightarrow \nu_e$ searches. The design of a such new facility will demand higher neutrino fluxes, a neutrino beam optimized to the atmospheric Δm^2_{23} and a detector optimized to efficiently detect electrons

and reject π°'s.

The T2K (Tokai to Kamioka) experiment (22) will aim neutrinos from the Tokai site of J-PARC (30 GeV, 0.75 MW) to the Super-Kamiokande detector 295 km away. The neutrino beam is situated at an off-axis angle of 2.5 degrees, ensuring a pion decay peak energy of about 0.6 GeV. The beam line is equipped with a set of dedicated on-axis (INGRID) and off-axis (ND280) near detectors at a distance of 280 m. It is expected that the sensitivity of the experiment in a five-year ν_μ run at the full J-PARC beam intensity, will be of the order of $\sin^2 2\theta_{13} \leq 0.006$ (90% CL). T2K is scheduled to begin data taking on January 2010.

The NOνA experiment with an upgraded NuMI off-axis neutrino beam (23) ($E_\nu \sim 2$ GeV and a ν_e contamination lower than 0.5%), a totally active 15 kton liquid scintillator detector and with a baseline of 810 km (12 km off-axis), has been approved at FNAL with the aim to explore $\nu_\mu \rightarrow \nu_e$ oscillations with a sensitivity 10 times better than MINOS.

1.2.3 Reactor experiments Another approach to searching for non-vanishing θ_{13} is to look at $\overline{\nu}_e$ disappearance using nuclear reactors as neutrino sources.

The Double Chooz (24) experiment, the follow-up to CHOOZ , will employ a far detector in the same location as the former CHOOZ detector as well as a near detector. The sensitivity after five years of data taking will be $\sin^2 2\theta_{13} = 0.025$ at 90% CL (24), which could be achieved as early as 2012.

The Daya Bay project in China (25) could reach a $\sin^2 2\theta_{13}$ sensitivity below 0.01 integrating 70 times the statistics of Double Chooz .

A sketch of θ_{13} sensitivities as a function of the time, following the schedule reported in the experimental proposals, is reported in Fig. 2.

1.2.4 Neutrino Super Beams Consensus exists that even a global fit of T2K plus NOνA plus reactors, will not be able to provide firm results (3σ or better) about leptonic CP violation (27) or sign(Δm^2_{23}) (28) whatever the value of θ_{13}. A further generation of long-baseline neutrino experiments will be needed to address this very important search in physics. The rule of thumb in such experiments is that they should be at least one order of magnitude more sensitive than T2K or NOνA . As a result they need an increase of two orders of magnitude on neutrino statistics requiring a consequent important reduction of systematic errors.

To fulfill such a challenging improvement, conventional neutrino beams must be pushed to their ultimate limits (neutrino super beams) (29) and gigantic (megaton scale) neutrino detectors must be built.

Phase II of the T2K experiment, often called T2HK (32), foresees an increase of beam power up to the maximum feasible with the accelerator and target (4 MW beam power), antineutrino runs, and a very large, 520 kt, water Čerenkov, HyperKamiokande or HK, to be built close to SuperKamiokande.

An evolution of T2HK is the T2KK (33) project, where half of the HK detector would be installed in Japan, while the second half would be mounted in Korea, at a baseline of about 900 km, around the second oscillation maximum.

1.2.5 CERN-SPL The CERN-SPL super beam is describe in a little more detail for its possible synergy with the CERN-Fréjus beta beam, as discussed in 2.6. In the CERN-SPL super beam project (34) the planned 4MW SPL (Superconducting Proton Linac) would deliver a 3.5 GeV/c H^- beam on a Hg target to

generate a neutrino beam with an average energy of ~ 0.3 GeV [1].

The ν_e contamination from K will be suppressed by threshold effects and the resulting ν_e/ν_μ ratio ($\sim 0.4\%$) will be known within 2% error. The use of a near and far detector (the latter at $L = 130$ km in the Fréjus area) will allow for both ν_μ-disappearance and $\nu_\mu \rightarrow \nu_e$ appearance studies. The physics potential of the SPL super beam (SPL-SB) with a water Čerenkov far detector with a fiducial mass of 440 kt, has been extensively studied (36, 37). The most updated sensitivity estimations for this setup have been published in Ref. (38) and are shown in Section **??**.

The MEMPHYS (Megaton Mass Physics) detector (41) is a megaton-class water Čerenkov designed to be located at Fréjus, 130 km from CERN, addressing both the non-accelerator domain (nucleon decay, SuperNovae neutrino from burst event or from relic explosion, solar and atmospheric neutrinos) and the accelerator (super beam, beta beam) domain (39).

1.3 New Concepts on Neutrino Beams

The intrinsic limitations of conventional neutrino beams can be overcome if the neutrino parents are fully selected, collimated and accelerated to a given energy.

This can be attempted within the muon lifetime, bringing to the neutrino factories (42), or within beta decaying ion lifetimes, bringing to the beta beam(43).

With this challenging approach several important improvements can be made to conventional neutrino beams:

[1] At present SPL is foreseen as one of the elements of a new injection chain for the SPS , in view of the LHC luminosity upgrades (35). In this context a power of 0.4 MW would be enough. Extensions to 4 MW could be driven by the needs of a neutrino super beam or a proton driver for a neutrino factory and/or a proton driver for EURISOL .

- The neutrino fluxes would be simply derived from the knowledge of the number of parents circulating in the decay ring and from their Lorentz boost factor γ.
- The energy shape of the neutrino beam would be defined by just two parameters, the end-point energy Q_β of the beta decaying parent and its Lorentz boost factor γ.
- The intrinsic neutrino backgrounds would be suppressed (in the case of beta beam) or reduced to wrong sign muons (golden channel in neutrino factories).

The technological problems derive from the fact that the parents need to be unstable particles, requiring a fast, efficient acceleration scheme.

2 CERN-FRÉJUS BETA BEAM PHYSICS POTENTIAL

2.1 General principles

A beta beam is produced from the decay of a high energy radioactive ion beam, resulting in a pure ν_e or $\bar{\nu}_e$ beam. The flavor transitions that can, in principle, be studied in this facility are:

$$\nu_e \to \nu_\mu \qquad \nu_e \to \nu_e \qquad \nu_e \to \nu_\tau$$

$$\bar{\nu}_e \to \bar{\nu}_\mu \qquad \bar{\nu}_e \to \bar{\nu}_e \qquad \bar{\nu}_e \to \bar{\nu}_\tau.$$

In the laboratory frame, the neutrino flux, $\Phi^{\rm lab}$, is given by (83):

$$\left.\frac{d\Phi^{\rm lab}}{dSdy}\right|_{\theta\simeq 0} \simeq \frac{N_\beta}{\pi L^2}\frac{\gamma^2}{g(y_e)} y^2(1-y)\sqrt{(1-y)^2-y_e^2} \tag{4}$$

where N_β is the number of ion decays per unit time, Q_β is the endpoint kinetic energy of the beta particle, γ is the relativistic Lorentz boost factor, m_e is the

mass of the electron, dS is the element of solid angle, L is the distance between the decay ring and the detector, $0 \leq y = \frac{E_\nu}{2\gamma Q_\beta} \leq 1 - y_e$, and $y_e = m_e/Q_\beta$; and

$$g(y_e) \equiv \frac{1}{60}\left\{\sqrt{1-y_e^2}(2-9y_e^2-8y_e^4) + 15y_e^4 \log\left[\frac{y_e}{1-\sqrt{1-y_e^2}}\right]\right\} \tag{5}$$

The intensity and the energy shape of the neutrino beam are determined by just four quantities: N_β, Q_β, γ, L. Once these parameters are fixed, the neutrino flux can be calculated precisely since the kinematics of β decay is very well-known (85).

There are some approximative scaling laws at the varying of the parameters (assuming N_β constant): the maximum γ to which a given accelerator can accelerate a ion is proportional to Z/A. For instance, if SPS can accelerate protons up to 450 GeV, ^{6}He $(Z/A = 2/6)$ can be accelerated up to $\gamma = 150$.

The neutrino flux Φ at a far detector placed at a distance L is:

$$\Phi \propto \frac{\gamma^2}{L^2}$$

because the emission angle of the neutrino from the parent ion, in the laboratory frame, is proportional to γ^{-1}.

Since the optimal distance L is defined by the oscillation Δm^2: $L \propto E_\nu/\Delta m^2$ and $E_\nu \propto \gamma Q_\beta$ the flux becomes

$$\Phi \propto \frac{(\Delta m^2)^2}{Q_\beta^2}.$$

Considering that the neutrino interaction rate I at the far detector is $I = \sigma\Phi$ and that the neutrino cross section σ goes as $\sigma \propto E_\nu$ (this scaling law becomes inaccurate for $E_\nu < 5$ GeV) a merit factor $\mathcal{M}$ can be derived

$$\mathcal{M} \propto \frac{\gamma}{Q_\beta}. \tag{6}$$

It follows that performances of a beta beam scale as the Lorentz boost factor γ and are inversely proportional to the endpoint energy Q_β of the parent ions.

2.2 The CERN-Fréjus Configuration

The CERN beta beam can accelerate ^{6}He ions up to $\gamma = 150$ and ^{18}Ne ions up to $\gamma = 250$. Given the characteristics of the ^{6}He decay, this translates to mean neutrino energies of up to ~ 600 MeV, equivalent to a maximum baseline of 300 km.

The only realistic candidate site for the excavation of a megaton class detector fitting this request is the Fréjus site, at a distance of 130 km.

To fit this distance the optimal γ for ^{6}He is $\gamma \simeq 100$. Higher γ values would increase interaction rates in the detector, but not the oscillated event interaction rates by very much, since the baseline would no longer fit the oscillation pattern. Furthermore background rates would rise, as discussed in Section 2.3.2.

Smaller γ values would have the advantage of suppressing background rates in the detector, $\gamma_{^6\mathrm{He}} = 66$ had been indeed the initial choice for the CERN-Fréjus configuration (86, 87) for this reason. Under this condition however the neutrino flux is smaller and a bigger fraction of ν_μ events created by oscillations produces a muon below the Čerenkov light production threshold ($p_\mu > 120$ MeV/c).

The CERN-Fréjus configuration (CFBB) is not designed to be the absolute optimal configuration for a beta beam experiment. It is intended to be a realistic setup where both the beam and the detector sites are chosen among realistic conditions.

2.3 Data Analysis

The most sensitive process in a beta beam experiment are $\nu_e \rightarrow \nu_\mu$ transitions as will be discussed in Section 2.4.

They introduce an experimental problem never faced so far, the detection of a

small content of ν_μ events in a pure ν_e beam. This process can be complemented by $\nu_e \to \nu_e$ transitions, where a small deficit in ν_e spectrum is looked for.

The combination of the two processes demands a detector capable of measuring with precision and high purity both electrons and muons. Furthermore to achieve good sensitivities for leptonic CP violation, the detector should be massive, in principle several units of 100 kt: the water Čerenkov technology, following the extremely successful experience of Super-Kamiokande, is the default choice for such a detector.

The main problematics of this kind of experiment and the different experimental approaches that have been proposed to attack the problem will be discussed in the next sections.

2.3.1 Signals The neutrino flux in this setup is shown in Fig. 3.

In this energy range almost all the neutrino charged-current interactions are quasi-elastic interactions (QE), a two-body configuration very favorable for a water Čerenkov detector because the neutrino energy can be derived by just measuring the momentum and the direction of the outgoing lepton. The precision in measuring the neutrino energy is shown in Fig 4. The energy of single ring non-quasi-elastic events results underestimated, because of the different kinematics. This effect is hardly visible in the low energy bins, where the non-quasi-elastic event fraction is small. The non-gaussian features of energy reconstruction are taken into account by using migration matrices connecting true and reconstructed neutrino energy, as discused in (38).

Data reduction is shown in Fig. 5 for ^{18}Ne events.

2.3.2 Backgrounds While a beta beam provides an absolutely clean beam of $\nu_e(\overline{\nu}_e)$, backgrounds can be produced by imperfect performances of the neutrino

detector.

The experimental sensitivity requires that the electron-muon mis-identification rate in the detector must be kept below 10^{-4}. A water Čerenkov detector is particularly efficient in this aspect, basing its rejection on two powerful handles. First muon and electron events have very different topologies in the detector, the former producing a rather sharp ring, the latter a rather fuzzy ring. Furthermore a muon can be positively identified by detecting its decay products: a Michel electron of energy up to $m_\mu/2$ with a characteristic time delay given by the muon lifetime (the probability for a negative muon to be captured before decay is 22% in water). A muon rejection factor of the order of 10^{-5} can be reached by these alghoritms.

The charged pions produced in the process

$$\nu N \rightarrow \Delta \rightarrow N\pi$$

where N is a generic nucleon and the charges are not specified, can be mis-identified as muons, generating backgrounds. At the energies typical of a beta beam, the momentum of these pions is such that the identification is very inefficient.

At the CERN Fréjus energies anyway the pion production is suppressed just because to produce a Δ the incident neutrino must have a momentum greater than 337 MeV/c, neglecting the nucleon Fermi motion, and the outgoing pion, to be detectable in water, must have a momentum greater than 159 MeV/c. Furthermore the probability that a negative pion be absorbed before the completion of its decay chain is quite high.

Atmospheric neutrinos are another source of background in a beta beam experiment. The spectrum of ν_μ and $\overline{\nu}_\mu$, shown in Fig. 3 right, overlaps the spectrum of oscillated signals, providing a copious source of backgrounds. The direction

of the outgouing muon is not a strong enough constraint to eliminate this background because both the quasi-elastic kinematics and the Fermi motion generate a loose correlation between the outgoing lepton and the incoming neutrino. At the energies of the $\gamma = 100$ beta beam, the angular resolution is about 0.25 radians. So the only other handle against atmospheric neutrinos is to keep the time in which beam neutrinos arrive to the detector very short, in other terms the duty cycle of the beta beam decay ring must be very short. As computed in (88) a duty cycle of 10^{-2} is needed to keep the atmospheric neutrino background rate below the NC pion background rate.

At higher γ the constraint on duty cycle relaxes because the atmospheric fluxes are less intense and the angular correlation tighter. This should help in loosening this constraint. It is worth noting that the fraction of background events with respect to the fully oscillated sample, after the analysis selection, is about 0.2%, well below the $\sim 1\%$ characteristic of super beam experiments. Furthermore these backgrounds (Fig. 5) have a different spectral distribution from oscillated events, reducing their impact on oscillation analysis, as will be discussed in Section 2.4.1.

2.4 Oscillation Analysis

In the following the CERN-Fréjus beta beam capabilities in measuring oscillation processes will be discussed. Most of the results shown in the following are taken from (38).

The default parameters used in the following are listed in Table 2. A prior knowledge of the oscillation parameters is included with an accuracy of 10% for θ_{12}, θ_{23}, Δm^2_{31}, and 4% for Δm^2_{21} at 1σ.

2.4.1 $\boldsymbol{\theta_{13}}$ SEARCHES Non-zero values of θ_{13} are looked for by exploiting $\nu_e \rightarrow \nu_\mu$ transitions. Following Eq. (1), $\nu_e \rightarrow \nu_\mu$ transitions can occur even for null values of θ_{13} , thanks to the contribution of the "solar" terms.

Systematic errors do not play a major role in these searches, where the important features are a high rate of neutrino events and a low rate of background events.

From Eq. (1) it can be also noted that the value of $\delta_{\rm CP}$ can greatly influence the sensitivity to θ_{13} . This suggests a combined run with neutrinos and antineutrinos (where the $\delta_{\rm CP}$ effect is opposite sign) to reduce such an influence.

Degenerate solutions do not influence θ_{13} sensitivity very much, for the simple fact that for very small θ_{13} these degenerate solutions disappear.

The discovery limits are shown in Fig. 6.

The beta beam performance depends crucially on the neutrino flux intensity, as can be seen from the dashed curves in Fig. 6, which has been obtained by reducing the number of ion decays/yr by a factor of two with respect to our standard values given in Tab. 2. In this case the sensitivity decreases significantly.

In Fig. 6 are illustrated also the effects of systematical errors on the θ_{13} discovery reach. The lower boundary of the band for each experiment corresponds to a systematical error of 2%, whereas the upper boundary is obtained for 5%. These errors include the (uncorrelated) normalization uncertainties on the signal as well as on the background, where the crucial uncertainty is the error on the background (38).

Also $\nu_e \rightarrow \nu_e$ transitions contribute to the θ_{13} sensitivity. They are however marginal if the overall systematic error is around 2% (as a comparison reactor experiments plan to reach systematic errors of about 0.2% in $\overline{\nu}_e$ disappearance just

to reach sensitivities of $\sin^2 2\theta_{13} \simeq 0.01$). As computed in (37), the CFBB experiment could reach sensitivities of $\sin^2 2\theta_{13} \leq 0.02$ (90% CL) to ν_e disappearance. Such values, compared to the sensitivity of Fig. 6, are clearly marginal.

2.4.2 Leptonic CP violation searches Leptonic CP violation searches are performed by comparing event rates and spectra in neutrino and antineutrino runs, as discussed in Section 1.1.1.

It is important to note that in the specific setup of CFBB, where matter effects are negligible and so no process is in competition with LCPV to generate differences between neutrino and antineutrinos, the simple comparison of neutrino and antineutrino oscillation rates can provide evidence of LCPV independently from any neutrino oscillation model.

For relatively large values of θ_{13} (say $\sin^2 2\theta_{13} > 0.01$), signal event rates are rather large, while the asymmetry between neutrino and antineutrino rates is relatively small. In this condition background rates are not that important and the dominant factor is systematic errors. For relatively small values of θ_{13} , signal rates are small, while the asymmetry is large. Under this condition systematic errors are less important, while background rates become an issue.

The LCPV discovery potential is shown in Fig. 8 where the widths of the bands in Fig. 8 correspond to different values of the systematical errors; it turns out that the most relevant uncertainty is the background normalization. The impact of systematics is very small, one finds that systematical errors dominate ($\sigma_{\rm bkgr}\sqrt{B} > 1$) if $\sigma_{\rm bkgr} \gtrsim 6\%$.

As discussed in (38). the true hierarchy and octant have a rather small impact on the LCPV sensitivity. In particular the sensitivity to maximal LCPV is completely independent.

2.5 Combined Analyses with the Atmospheric Neutrinos

Beta beam and atmospheric neutrino data are a truly synergic combination, in that together the two samples provide more information than expected just from statistics.

Beta beam has very limited capabilities in measuring sign(Δm^2_{23})and resolving degeneracies on the other hand atmospheric neutrinos, even if measured with large statistics, cannot measure sign(Δm^2_{23})in the absence of a measured value of θ_{13} , precisely what beta beam measures at best.

The power of a combination of LBL experiments based on megaton scale water Čerenkov detectors with data from atmospheric neutrinos (ATM) has been pointed out in (89).

A detailed computation of the beta beam+ATM analysis has been performed in (38), where the ATM analysis was tailored to the characteristics of the MEMPHYS detector, whose bigger dimensions with respect to Super-Kamiokande allow for the containment of events of higher energy. Also multi-ring events, defined as fully contained charged-current events which are not tagged as single-ring, are included in the analysis.

The combination of ATM+beta beam data leads to a non-trivial sensitivity to the neutrino mass hierarchy, i.e. to the sign of Δm^2_{31} as shown in Fig. 9. For beta beam data alone (dashed curves) there is practically no sensitivity in the CFBB setup (because of the very small matter effects due to the relatively short baseline). However, by including data from atmospheric neutrinos (solid curves) the mass hierarchy can be identified at 2σ CL provided $\sin^2 2\theta_{13} \gtrsim 0.02 - 0.03$. Fig. 9 is computed with a true value of $\theta_{23} = \pi/4$. Generically the hierarchy sensitivity increases with increasing θ_{23}, see (89) for a detailed discussion.

The effect of the atmospheric data in breaking degeneracies has been discussed in (38).

2.6 Combined Analyses with the SPL Super Beam

Soon after the first proposal of beta beams (43) it was realized that neutrinos created by the SPL could be fired to the same detector (37).

The injector of a beta-beam complex must be a 1 - 3 GeV Linac, precisely the energy of the SPL. Furthermore radioactive ion production requires at most 0.2 MW, while SPL could deliver up to 4 MW of power.

Under these circumstances a very intense super beam, already discussed in Section 1.2.5, can run together with a beta beam. The typical energy of a neutrino beam created by the SPL can nicely match the energy of a $\gamma = 100$ beta beam (see Fig. 3) so the two neutrino beams can share the same baseline, thus the same detector.

The combination of a super beam with a beta beam in the same experiment can provide an experimental environment with very unique characteristics:

- The two beams can be used to separately study CP channels like $\nu_\mu \to \nu_e$ vs $\overline{\nu}_\mu \to \overline{\nu}_e$ and $\nu_e \to \nu_\mu$ vs $\overline{\nu}_e \to \overline{\nu}_\mu$.
- They can be mixed to study T transitions like $\nu_\mu \to \nu_e$ vs $\nu_e \to \nu_\mu$ and $\overline{\nu}_\mu \to \overline{\nu}_e$ vs $\overline{\nu}_e \to \overline{\nu}_\mu$.
- The can be mixed to study CPT transitions like $\nu_\mu \to \nu_e$ vs $\overline{\nu}_e \to \overline{\nu}_\mu$ and $\nu_e \to \nu_\mu$ vs $\overline{\nu}_\mu \to \overline{\nu}_e$.

The addition of a super beam to a beta beam could also complement some of the weak points of the beta beam, namely the lack of sensitivity to the atmospheric parameters θ_{23} and Δm^2_{23} and the lack of ν_μ events in the close detector, useful

for calibrating beta beam signal efficiency and measuring the ν_e/ν_μcross section ratio.

In an SPL super beam+beta beam experiment all the channels would be measured in the same detector with small background rates. This is highly beneficial for systematic errors and would provide redundancy in the oscillation signals, a feature that should not be underestimated in an experimental field that today is completely unexplored.

3 PHYSICS POTENTIAL OF OTHER BETA BEAM SETTINGS

Several different new concepts have been published to explore the full capabilities of a beta beam setup.

High energy beta beamcapable of improving the CFBB performances will be discussed in section 3.1. Beta beams based on different ions than ^{6}He$\,/^{18}$Ne$\,$, chosend to have a higher Q_β value and so to produce higher energy neutrino beams for the same accelerator setup are discussed in section 3.2.

Beta beams based on electron capture processes of radioactive ions, rather than on their beta decays, producing monochromatic neutrino beams will be presented in section 3.3.

To conclude, the physics potential of low energy beata beams, focussed on studies of neutrino properties rather than on neutrino oscillations, will be discussed in section 3.4.

3.1 High Energy Beta Beams

High energy beta beams (HEBB) have been introduced by (83), where the final accelerator is designed to accelerate ^{6}He up to $\gamma = 350$ (2.3 times higher that the

maximum $\gamma(^6\mathrm{He})$ reachable at the SPS), a condition fulfilled by an accelerator capable of accelerating protons at 1 TeV. The same number of ion decays/year as the CFBB has been considered.

Two major upgrades of the accelerator scheme are needed for high energy beta beams. Of course a new accelerator is needed. Proton accelerators at 1 TeV energy have been recently dismantled (HERA at Desy) or are going to be shut-down (Tevatron at Fermilab). The LHC is a collider with a very slow acceleration cycle which makes it unsuitable for the acceleration of the large number of radioactive ions required for a beta beam. A possible energy upgrade of the LHC would require a new higher energy injector, SPS+ (35), which could be used for a higher energy beta-beam.

Also the decay ring is heavily affected by a γ increase of the stored ions. First its length scales linearly with γ, since the magnetic rigidity of the ions is proportional to γ and the fraction of length of the straight decay section cannot be reduced without compromising the neutrino fluxes at the far detector. Second this long decay ring must be built at the right slope to point to the far detector. Considering a baseline of 650 km, the slope would be of about 3°, such that a 7 km long decay ring would end up at a depth of about 200 m [2]. Third the number of ions stored in the decay ring scales again with γ, according to the Lorentz boost on their lifetime.

An important advantage of a high energy beta beam is the possibility to increase the baseline length to the point where sensitivity to sign(Δm^2_{23}) becomes sizable.

[2] In the Cern Fréjus case the slope would be of 0.2° taking into consideration the differenc of altitude between CERN (400 m) and the Fréjus lab (1200 m)

Reference (90) studies the case of a water Čerenkov detector at $\gamma = 350$ for ^{6}He and ^{18}Ne ions. In a water Čerenkov detector only quasi-elastic (QE) events can be properly reconstructed (see section 2.3.1), so by increasing the average neutrino energy, the fraction of well reconstructed events decreases, until the point where the flux increase provided by the higher gamma is vanished by the loss of QE events. According to (90) this happens for $\gamma \simeq 400$.

Backgrounds from NC are much more in HEBB than in CFBB, but they cluster at small energies. As demonstrated by Ref. (90), a simple lower cut in the visible energy keeps NC backgrounds to a tolerable level. Also atmospheric neutrinos integrated in the signal energy range increase, but much less than signal events, when compared to CFBB. This feature implies that in HEBB the bounds to the beta beam duty cycle derived from the atmospheric neutrino background rate are less severe, allowing for higher duty cycles.

Following the results of (90) a $\gamma = 350$ beta beam would have marginal improvement as far as θ_{13} and LCPV sensitivities are concerned with respect to an SPS-based beta beam at the maximum γ ($\gamma = 150$ for ^{6}He and ^{18}Ne) and at the optimal baseline (L=300 km) [3], while $\gamma = 350$ has definitely better performances as far as sign(Δm^2_{23}) sensitivity is concerned.

As emerges from the above discussion, a water Čerenkov detector shows some limitation in the energy range of high energy beta beam, if only quasi-elastic events can be efficiently reconstructed. To overcome this problem different detector technologies have been taken into account for HEBB.

In (91), the case of a totally active scintillating detector (TASD), derived from

[3] This is the right way to compare the two options, by fixing the optimal baseline in the two cases. The problem is then the practical possibility of actually having a megaton class detector at the right depth at the optimal baseline.

the NOνA project, has been considered. An interesting study of (91) is the scaling of performances with the number of ion decays/year. Assuming a scaling law as:

$$N^i = N_0 \cdot (\frac{\gamma_0}{\gamma})^n \tag{7}$$

where N (N_0) is the number of decays/year at a given γ (γ_0), and γ_0 is a reference point. $n = 0$ is the case of constant ion decays/year, while $n = 1$ is the case of "constant power" in the accelerator. In this latter case the sensitivity of the setup becomes rather independent from γ, showing that the assumptions about this scaling law are very important for the overall comparisons.

A different detector technology has been considered in (92): an iron calorimeter, where the sensitive elements (2 cm thick glass RPC planes with a 2 mm gas filled gap) are interleaved with iron plates (4 cm thick). This configuration has the advantage of providing a higher density than a TASD detector, such that a 40 kt detector could fit a present LNGS hall, a very attractive experimental situation. A full simulation of this detector has been performed, allowing for a robust sensitivity estimation. The fraction of NC backgrounds with respect to the non-oscillated ν_e events is 8.8×10^{-3} at $\gamma = 580$, a much higher rate than the 10^{-3} rate assumed (but not computed) at $\gamma = 500$ for a TASD detector.

Overall performances of this setup almost match those of the CERN-Fréjus scenario, again assuming a constant ion decay rate. Combined sensitivity with atmospheric neutrinos of this setup have been also studied in (92) showing that its sensitivity, as expected from the longer baseline, outperforms CFBB performances as far as concerns sign(Δm^2_{23}).

3.2 Beta Beams Based on ^{8}B and ^{8}Li Ions

^{8}B and ^{8}Li ions have a significantly higher Q_β value than ^{6}He and ^{18}Ne as can be derived from Table 3. In Section 2.1 it has already been shown that higher Q_β ions can allow greater neutrino energies for the same γ:

$$E_\nu^{\max} = 2\gamma Q_\beta \tag{8}$$

Furthermore the Z/A of the ^{8}B /^{8}Li ions are higher than the formers': such that considering the β^- emitters they could produce a neutrino beam 4.74 times more energetic than a ^{6}He /^{18}Ne beam, for the same accelerator energy, with a shorter decay ring length. On the other hand the merit factor of a ^{8}B /^{8}Li beam (see Section 2.1) is smaller than a ^{6}He /^{18}Ne beam since it is inversely proportional to Q_β and so it would produce smaller fluxes at the same neutrino energy; it would need about four times more ions to match the performances of CFBB.

In (51), as discussed in Section **??**, an innovative procedure has been proposed to produce ^{8}B /^{8}Li ions, in principle capable of producing 2 - 3 orders of magnitude more radioactive ion fluxes. Feasibility and performances of this injection scheme will be studied in the context of the European Design Study EuroNu (**?**).

The physics case of a ^{8}B /^{8}Li beta beam based on the Fermilab Main Injector has been discussed in (96).

The authors of (97) have studied the case of a mixed ^{8}B /^{8}Li and ^{6}He /^{18}Ne beta beam, based on SPS. A 500 kt water Čerenkov detector with a baseline of about 700 km would receive the ^{8}B /^{8}Li beta beam at the first oscillation maximum and the ^{6}He /^{18}Ne beta beam at the second oscillation maximum. The same ion decays/year of CFBB are assumed also for ^{8}B and ^{8}Li . This combination of first/second maximum is very powerful in solving degeneracies, since the

differences between the oscillation patterns of the different oscillation components are more and more visible with the development of oscillations. Nevertheless at the second oscillation maximum fluxes are reduced by about one order of magnitude, and statistics is the major component in sensitivity to θ_{13} and LCPV. Therefore this has little advantage as far as θ_{13} and LCPV are concerned, while it outperforms CFBB as far as sign(Δm^2_{23}) sensitivity is concerned.

Along this line it is also interesting to note the study of reference (98) where the case of a single ^{18}Ne exposure is considered at $\gamma = 450$ (within the reach of the SPS+) and with a 50 kt iron detector placed at a baseline of 1050 km (CERN-Boulby mine). This neutrino-only setup would cover both the first and the second oscillation maximum. While the θ_{13} , LCPV and sign(Δm^2_{23}) sensitivities do not ouperform those of other beta beam setups, this particular scheme could reach an interesting sensitivity to the octant of θ_{23} .

The combination of high energy, ^{8}B /^{8}Li based, beta beams allows the so called "magic baseline" $L_{\rm magic}$ to be covered.

The concept of a magic baseline (10, 99) derives from the observation that in Eq.(1) for $\rho L = \sqrt{2}\pi/G_F Y_e$ (Y_e is the electron fraction inside the earth) any $\delta_{\rm CP}$ dependence disappears from $P_{e\mu}$ allowing sign(Δm^2_{23}) effects to be measured without any degenerate solution.

The measurement of neutrino oscillation at the magic baseline is the ideal complement to LCPV searches, since it decouples fake CP effects generated by matter effects from the genuine CP effects looked for in LCPV searches.

According to the Preliminary Reference Earth Model PREM (100) earth matter density profile, $L_{\rm magic} \simeq 7690$ km, the resonance energy for matter effects would

be:

$$E_{\rm res} \equiv \frac{|\Delta m^2_{31}| \cos 2\theta_{13}}{2\sqrt{2} G_F N_e} \simeq 7 \text{ GeV} \tag{9}$$

for $|\Delta m^2_{31}| = 2.4 \cdot 10^{-3}$ eV^2 and $\sin^2 2\theta_{13} = 0.1$.

It is important to note that close to matter resonance, the flux of oscillated events at the detector roughly falls as a function of $1/L$ (against the $1/L^2$ fall of vacuum oscillations), which means that longer baselines might be preferred.

Studies of beta beams at the magic baselines have been initiated (101) within the context of the India-based Neutrino Observatory (INO) (102), where a large magnetized iron calorimeter (ICAL) is set to come up. The CERN-INO distance approaches the magic baseline, being 7152 km. It has to be noted anyway that the slope at which the decay ring should be built to point at a 7000 km far detector is about 34.5°, such that it seems almost impossible to built it.

Two detectors at two different distances are anyway needed, since the detector at the magic baseline is blind to any LCPV effect by construction, this kind of setup has been studied in (103–105)

In these studies the performances of the INO detector are parameterized in the absence of a full simulation and kept constant in the whole energy range studied in the paper. In particular NC rejection cannot be constant at different neutrino energies, and the 10^{-4} NC rejection factor considered in the paper is in disagreement with the rejection factor computed with a full simulation in (92).

The potentialities of a high-γ-high-Q beta beam are anyeay extremely competitive ().

3.3 Monochromatic Neutrino Beams

Monochromatic neutrino beams based on the electron capture process (ECB) are certainly an intriguing experimental setup, but for LCPV searches they have two major apparent limitations: there is no way to have antineutrino beams (a conceptual possibility for the production of monochromatic neutrino beams is discussed later in this section) and they miss spectral information, which is very important to solve degeneracies.

To overcome these limitations interesting experimental strategies have been introduced.

In (76, 93) it has been proposed to study θ_{13} and LCPV in a ECB setup based on the ^{150}Dy ion (3.1 min lifetime and $Q = 1794$ keV) running the beam at two γs tuned to the first and the second oscillation maximum. Two setups are considered, the first, based on the SPS and the CERN-Fréjus baseline, would run the ions at $\gamma = 90$ and $\gamma = 195$ the second, based on SPS+, considers $\gamma = 195$, 440. The detector is a water Čerenkov of 440 kt in both cases. Performances of ECB in these configurations are very promising. It should anyway be noted that in this study any background contamination has been neglected and 100% signal efficiency has been assumed, a quite optimistic scenario.

Reference (94) proposes a more aggressive strategy. based on $^{110}_{50}Sn$ isotopes with $Q = 267$ Kev and a 4.11 h lifetime. Running these ions at $\gamma = 2500$ and a baseline of 600 km, the energy of events at $R = 100$ m would have a 15% smaller energy than events at $R = 0$. The vertex resolution of a water Čerenkov detector, about 30 cm, is suitable for such a measurement. The requirements of beam divergence $p_x/p_z \leq 1$ μrad, and an equivalent precision of the absolute beam direction seem anyway very challenging.

A way to generate monochromatic antineutrino beams has been delineated in (79) (see also Section **??**). It is based on the process of the bound-state β decay (95) where the electron is created in a previously unoccupied bound atomic state and the antineutrino is emitted at a fixed energy. Candidates exist like ${}^{108}_{47}Ag^{46+}$ with $\tau_{1/2} = 24.4$ s and neutrino energies of 1.90 and 1.67 MeV for the EC and bound-beta lines respectively, but it should be noted that the branching ratios for such processes are of about 1%, making it very difficult even conceptually to produce significative neutrino fluxes.

3.4 Low Energy Beta Beams

Beta beams are the ideal tool for measuring neutrino cross sections, since the neutrino beam flux can be predicted with high precision. This particular feature has been extensively discussed in the literature for neutrino energies around 100 MeV, where a wide set of interesting non-oscillation neutrino experiments is possible.

In (109) it was proposed to build a low energy facility in the 100 MeV energy range for nuclear structure studies and neutrino-nucleus interactions (109–113), electroweak tests of the Standard Model (109, 114–116) as well as core-collapse Supernova physics (109, 117, 119).

In this energy range the decay ring characteristics and the detector locations have to be re-optimized, as discussed in (109, 110, 120).

Neutrino-nucleus interactions represent a topic of current great interest for various domains of physics, from neutrino physics to nuclear physics and astrophysics. The motivations come for example from the need for a precise knowledge of the neutrino detector response in neutrino experiments and in core collapse

supernova observatories aiming at the detection of the relic supernova neutrino background (39) using neutrino interaction on argon (123) and carbon or oxygen (124) or of neutrinos from an (extra)galactic explosion (39).

For instance, the 1n or 2n emission associated with charged-current events in a supernova lead-based observatory depends on the average electron neutrino energy, which encodes information on the still unknown third neutrino mixing angle θ_{13} (125). Such a detector is now planned at SNOLAB (the HALO project).

Neutrino-nucleon reactions play a crucial role in the understanding of the supernova dynamics (126,127), the yields of the r-process nucleosynthesis that could take place in such environments (128) and also contribute to the energy transfer (from accretion-disk neutrinos to nucleons) in gamma-ray burst models (129,130). Finally, understanding the subtleties of the neutrino-nucleon interactions is important to the terrestrial observation of neutrino signals (131, 132).

Besides the astrophysical applications, a precise knowledge of the nuclear response of neutrinos is also crucial for our knowledge of the nuclear isospin and spin-isospin response that has fundamental implications, for example the search of physics beyond the Standard Model through neutrinoless double-beta decay (112).

Several applications for fundamental interaction studies of low energy beta beams have been discussed so far: the measurement of the Weinberg angle at low momentum transfer (115), a conserved vector current (CVC) test with neutrino beams (116), the measurement of the neutrino magnetic moment (111), the measurement of coherent neutrino-nucleus elastic scattering (134), the sensitivity to extra neutral gauge bosons, leptoquarks and r-parity breaking interactions (135).

For a more detailed discussion about physics at a low energy beta beam see

the topical review published by Cristina Volpe (118).

Literature Cited

1. T. Schwetz, M. Tortola and J. W. F. Valle, New J. Phys. **10**, 113011 (2008) [arXiv:0808.2016 [hep-ph]].
2. F. Feruglio, A. Strumia and F. Vissani, Nucl. Phys. B **637** (2002) 345 [Addendum-ibid. B **659** (2003) 359].
3. M. Fukugita and T. Yanagida, Phys. Lett. B **174** (1986) 45.
4. A. Blondel *et al.*, CERN-2004-002, ECFA-04-230.
5. Beams for European Neutrino Experiments (BENE): Midterm scientific report. By BENE Steering Group (A. Baldini *et al.*). Jan 2006.
6. A. Bandyopadhyay *et al.* [ISS Physics Working Group], Rept. Prog. Phys. **72** (2009) 106201 [arXiv:0710.4947 [hep-ph]].
7. J. Burguet-Castell, M. B. Gavela, J. J. Gomez-Cadenas, P. Hernandez and O. Mena, Nucl. Phys. B **608** (2001) 301.
8. H. Minakata and H. Nunokawa, JHEP **0110** (2001) 001.
9. G. L. Fogli and E. Lisi, Phys. Rev. D **54** (1996) 3667.
10. V. Barger, D. Marfatia and K. Whisnant, Phys. Rev. D **65** (2002) 073023.
11. M. G. Catanesi *et al.* [HARP Collaboration], Nucl. Instrum. Meth. A **571**, 527 (2007).
12. M. G. Catanesi *et al.* [HARP Collaboration], Nucl. Phys. B **732**, 1 (2006).
13. [HARP Collaboration], Eur. Phys. J. C **52**, 29 (2007) [arXiv:hep-ex/0702024]
14. P. Huber, M. Mezzetto and T. Schwetz, JHEP **0803**, 021 (2008) [arXiv:0711.2950 [hep-ph]].

15. M. Apollonio *et al.* [CHOOZ Collaboration], Eur. Phys. J. C **27** (2003) 331.
16. M. H. Ahn *et al.* [K2K Collaboration], Phys. Rev. Lett. **93** (2004) 051801.
17. The Fermilab NuMI Group, *NumI Facility Technical Design Report* Fermilab Report NuMI-346, 1998.
18. P. Adamson *et al.* [MINOS Collaboration], arXiv:0909.4996 [hep-ex].
19. OPERA Collaboration, CERN-SPSC-P-318, LNGS-P25-00; H. Pessard [OPERA Collaboration], arXiv:hep-ex/0504033.M. Guler *et al.* [OPERA Collaboration], CERN-SPSC-2000-028.
20. G. Acquistapace *et al.*, CERN 98-02, INFN/AE-98/05 (1998); CERN-SL/99-034(DI), INFN/AE-99/05 Addendum.
21. M. Komatsu, P. Migliozzi and F. Terranova, J. Phys. G **29** (2003) 443.
22. Y. Itow *et al.*, arXiv:hep-ex/0106019.
23. D. S. Ayres *et al.* [NOvA Collaboration], arXiv:hep-ex/0503053.
24. F. Ardellier *et al.* [Double Chooz Collaboration], arXiv:hep-ex/0606025.
25. X. Guo *et al.* [Daya Bay Collaboration], arXiv:hep-ex/0701029.
26. M. Mezzetto, arXiv:0905.2842 [hep-ph].
27. P. Huber, M. Lindner, M. Rolinec, T. Schwetz and W. Winter, Nucl. Phys. Proc. Suppl. **145** (2005) 190. P. Huber, M. Lindner, T. Schwetz and W. Winter, JHEP **0911** (2009) 044 [arXiv:0907.1896 [hep-ph]].
28. O. Mena, H. Nunokawa and S. J. Parke, Phys. Rev. D **75** (2007) 033002.
29. B. Richter, arXiv:hep-ph/0008222.
30. A. Guglielmi, M. Mezzetto, P. Migliozzi and F. Terranova, arXiv:hep-ph/0508034, published in D. Bettoni *et al.*, Phys. Rept. **434** (2006) 47.
31. A. Blondel, A. Cervera-Villanueva, A. Donini, P. Huber, M. Mezzetto and P. Strolin, Acta Phys. Polon. B **37** (2006) 2077.

32. T. Kobayashi, J. Phys. G 29, 1493 (2003).

33. T. Kajita, H. Minakata, S. Nakayama and H. Nunokawa, Phys. Rev. D **75** (2007) 013006. M. Ishitsuka, T. Kajita, H. Minakata and H. Nunokawa, Phys. Rev. D **72** (2005) 033003.

34. B. Autin *et al.*, CERN-2000-012. R. Garoby, CERN-AB-2005-007.

35. http://paf.web.cern.ch/paf/. O. Bruning *et al.*, CERN-LHC-PROJECT-REPORT-626; W. Scandale, Nucl. Phys. Proc. Suppl. **154** (2006) 101.

36. J. J. Gomez-Cadenas *et al.*, Proceedings of *Venice 2001, Neutrino telescopes* vol. 2*, 463-481 [arXiv:hep-ph/0105297]. A. Blondel *et al.*, Nucl. Instrum. Meth. A **503** (2001) 173. M. Mezzetto, J. Phys. G **29** (2003) 1771. M. Apollonio *et al.*, arXiv:hep-ph/0210192. J. E. Campagne and A. Cazes, Eur. Phys. J. C **45**, 643 (2006)

37. M. Mezzetto, Nucl. Phys. Proc. Suppl. **149** (2005) 179. J. E. Campagne, Nucl. Phys. Proc. Suppl. **155**, 185 (2006) [arXiv:hep-ex/0511013].

38. J. E. Campagne, M. Maltoni, M. Mezzetto and T. Schwetz, JHEP **0704** (2007) 003 [arXiv:hep-ph/0603172].

39. D. Autiero *et al.*, [arXiv:0705.0116].

40. M. V. Diwan *et al.*, Phys. Rev. D **68** (2003) 012002 M. Diwan *et al.*, arXiv:hep-ex/0608023.

41. A. de Bellefon *et al.*, arXiv:hep-ex/0607026.

42. S. Geer, Phys. Rev. D **57** (1998) 6989 [Erratum-ibid. D **59** (1999) 039903], [hep-ph/9712290].

43. P.Zucchelli, Phys. Let. B, **532** (2002) 166-172.

44. B.Autin, M. Benedikt, M. Grieser, S. Hancock, H. Haseroth, A. Jansson, U. Köster, M. Lindroos, S. Russenschuck and F. Wenander, CERN/PS 2002-

078 (OP), Nufact Note 121, Proceedings of Nufact 02, London, UK, 2002, J. Phys. G: Nucl. Part. Phys. 29 (2003) 1785-1795.

45. C. Albright, V. Barger, J. Beacom, S. Brice, J. J. Gomez-Cadenas, M. Goodman, D. Harris, P. Huber, A. Jansson, M. Lindner, O. Mena, P. Rapidis, K. Whisnant, W. Winter, C. Albright *et al*, in APS Joint Study Report on the Future of Neutrino Physics, FNAL-TM-2259, 2004; arXiv:physics/0411123.
46. H. R. Ravn and B. W. Allardyce, *On-Line Mass Separators, in Treatise on Heavy-Ion Science,* Edt. D. A. Bromley, Plenum Press, New York, 1989, ISBN 0-306-42949-7.
47. N. Thiollière, J. C. David, V. Blideanu, D. Doré, B. Rapp, D. Ridikas, *Optimization of 6He production using W or Ta converter surrounded by BeO target assembly,* Internal note CEA, DAPNIA-06-274 and EURISOL note, 03-25-2006-0004.
48. M. Hass, D. Berkovits, T.Y. Hirsh, V. Kumar, M. Lewitowicz and F. de-Oliveira, *Light radioisotopes for nuclear astrophysics and neutrino physics,* J. Physics **G35**, 104042 (2008).
49. E. Bouquerel, J. Lettry and T. Stora *BeO dual target prototype for 6He production - a preliminary note*, EURISOL internal note, http://eurisol.org.
50. M. Loislet and S. Mitrofanov, *Alternative production scenarios for* ^{6}*He and* ^{18}*Ne,* Oral presentation at the 6th Beta-beam Task Meeting, EURISOL, 19th November 2007, http://eurisol.org.
51. C. Rubbia, A. Ferrari, Y. Kadi and V. Vlachoudis, *Beam cooling with ionisation losses,* Nucl. Instrum. Meth. A **568** (2006) 475 [arXiv:hep-ph/0602032].
52. Y. Mori, *Development of FFAG accelerators and their applications for intense secondary particle production,* Nucl. Instrum. and Methods A, **562**

(2006) 591.

53. D. Neuffer, Fermi National Laboratory: Muon Collider and accelerator division document database: NFMCC-doc-516, beams-doc-2856 (2007).
54. C. Reed, J. Nolen, V. Novick, J. Specht, and Y. Momozaki, *A Liquid Lithium Thin Film Stripper for RIA*, in the proceedings the Seventh International Conference on Radioactive Nuclear Beams, Cortina d'Ampezzo, Italy, 2006.
55. P. Sortais, J. L. Bouly, J. C. Curdy, T. Lamy, P. Sole, T. Thuillier, J. L. Vieux-Rochaz, D. Voulot, *ECRIS development for stable and radioactive pulsed beams,* Rev. Sci. Instr. **75** (2004) 1610.
56. L. Hermansson and D. Reistad, *Electron cooling at CELSIUS,* Nucl. Instrum. Meth. A **441** (2000) 140.
57. E. Wilson, *An Introduction to Particle Accelerators, Oxford University Press,* Oxford, 2001, ISBN 0-19-850829-8.
58. P. N. Ostroumov, *Development of a medium-energy superconducting heavy-ion linac,* Phys. Rev. ST Acc. Beams 5 (2002) 030101.
59. The EURISOL report, APPENDIX D: Post-Accelerator & Mass Separator for EURISOL, Edt. M.-H. Moscatello, GANIL, Caen, France, 2003, EUROPEAN COMMISSION CONTRACT No. HPRI-CT-1999-500001.
60. L. J.Laslet and L. Resegotti, Proceedings of the 6th International Conference on High-Energy Accelerators, Cambridge, USA, p.150.
61. A. Lachaize, A. Tkatchenko, *The Rapid Cycling Synchrotron of the EURISOL Beta Beam facility,* EURISOL DS task note 12-25-2008-0012.
62. C. Omet et al, *Charge change-induced beam losses under dynamic vacuum conditions in ring accelerators,* New J. Phys. **8** (2006) 284, doi:10.1088/1367-2630/8/11/284

63. M. Magistris and M. Silari, *Parameters of radiological interest for a beta-beam decay ring,* CERN technical note, CERN-TIS-2003-017-RP-TN.

64. M. Kirk, *PS activation and collimation studies,* Oral presentation at the 6th Beta-beam Task Meeting, EURISOL, 19th November 2007, http://eurisol.org

65. A. Chancé and J. Payet, *Beta-beam decay ring design*, In the proceedings of EPAC, 2006, Edinburgh, UK, p.1933.

66. A. Chancé and J. Payet, *Transport of the decay products in the beta-beam decay ring,* In the proceedings of EPAC, 2008, Genoa, Italy. p.3104

67. M. Benedikt and S. Hancock, *A novel scheme for injection and stacking of radioactive ions at high energy,* Nucl. Instrum. Meth. A **550** (2005) 1.

68. F.W. Jones and E. Wildner, *Simulation of decays and secondary ion losses in a betabeam decay ring,* in the proceedings of PAC07, Albuquerque, New Mexico, USA

69. R. Gupta, M. Anerella, M. Harrison, J. Schmalzle and N. Mokhov, *Open midplane dipole design for LHC IR upgrade,* IEEE Trans. Appl. Supercond. **14** (2004) 259.

70. J. MacLachlan, *Particle Tracking in E-Phi Space for Synchrotron Design & Diagnosis,* Fermilab-CONF-92/333 (Nov. 92), presented at 12-th Int'l Conf. on Appl. of Acc. in Res. and Ind., Denton TX, 4 Nov 1992 and http://www-ap.fnal.gov/ESME/

71. S. Hancock, M. Lindroos, E. McIntosh and M. Metcalf, *Tomographic measurements of longitudinal phase space density,* Comput. Phys. Commun. **118** (1999) 61.

72. S. Hancock, *Technical challenges of the EURISOL beta-beam,* AIP Conf.

Proc. **981** (2008) 89.

73. http://snowmass2001.org/
74. A. Källberg and M. Lindroos, *Accumulation in a ring at low energy for the beta-beam*, EURISOL DS/TASK12/TN-05-04, http://eurisol.org and In the proceedings of European Particle Accelerator Conference, 2006, Edinburgh, Scotland.
75. M. Blaskiewicz and J. M. Brennan, *A Barrier Bucket Experiment for Accumulating De-bunched Beam in the AGS,* In the proceedings of the European Particle Accelerator Conference, Barcelona, Spain, 1996.
76. J. Bernabeu, J. Burguet-Castell, C. Espinoza and M. Lindroos, *Monochromatic neutrino beams,* JHEP **0512**, 014 (2005) [arXiv:hep-ph/0505054].
77. J. Sato, *Monoenergetic Neutrino Beam for Long-Baseline Experiments*, Phys. Rev. Lett. **95** (2005) 131804.
78. E. Nacher, *Beta decay studies in the $N \sim Z$ and the rare-earth regions using Total Absorption Spectroscopy techniques*, Ph. D. Thesis, Univ. Valencia (2004).
79. A. Fukumi, I. Nakano, H. Nanjo, N. Sasao, S. Sato, M. Yoshimura, *CP-even neutrino beam*, arXiv:hep-ex/0612047.
80. M. Lindroos, J. Bernabeu, J. Burguet-Castell and C. Espinoza, *A monochromatic electron neutrino beam,* In the proceedings of International Europhysics Conference on High energy Physics, Lisboa, Portugal, 2005, Proceedings of Science, http://pos.sissa.it/
81. F. Bosch, GSI, Germany, 2005, private communication.
82. W. Bambynek, H. Behrens, M. H. Chen, B. Crasemann, M. L. Fitzpatrick, K. W. D. Ledingham, H. Genz, M. Mutterer and R. L. Intemann, *Orbital*

electron capture by the nucleus, Rev. Mod. Phys. **49** (1977) 77.

83. J. Burguet-Castell, D. Casper, J. J. Gomez-Cadenas, P. Hernandez and F. Sanchez, Nucl. Phys. B **695** (2004) 217 [arXiv:hep-ph/0312068].
84. http://www.ganil.fr/eurisol/
85. See for instance S. S. Masood, S. Nasri, J. Schechter, M. A. Tortola, J. W. F. Valle and C. Weinheimer, Phys. Rev. C **76** (2007) 045501 [arXiv:0706.0897 [hep-ph]].
86. M. Mezzetto, J. Phys. G **29** (2003) 1771 [arXiv:hep-ex/0302007].
87. J. Bouchez, M. Lindroos and M. Mezzetto, AIP Conf. Proc. **721** (2004) 37 [arXiv:hep-ex/0310059].
88. M. Mezzetto, Nucl. Phys. Proc. Suppl. **155** (2006) 214
89. P. Huber, M. Maltoni and T. Schwetz, *Resolving parameter degeneracies in long-baseline experiments by atmospheric neutrino data,* Phys. Rev. D **71**, 053006 (2005) [arXiv:hep-ph/0501037]. R. Gandhi, P. Ghoshal, S. Goswami, P. Mehta and S. Uma Sankar, *Probing the nu mass hierarchy via atmospheric nu/mu + anti-nu/mu survival rates in Megaton water Cerenkov detectors,* arXiv:hep-ph/0506145.
90. J. Burguet-Castell, D. Casper, E. Couce, J. J. Gomez-Cadenas and P. Hernandez, Nucl. Phys. B **725**, 306 (2005)
91. P. Huber *et al.*, Phys. Rev. D **73**, 053002 (2006).
92. F. Terranova, A. Marotta, P. Migliozzi and M. Spinetti, Eur. Phys. J. C **38** (2004) 69. A. Donini, E. Fernandez-Martinez, P. Migliozzi, S. Rigolin, L. Scotto Lavina, T. Tabarelli de Fatis and F. Terranova, Eur. Phys. J. C **48**, 787 (2006)
93. J. Bernabeu and C. Espinoza, Phys. Lett. B **664**, 285 (2008)

[arXiv:0712.1034 [hep-ph]]. J. Bernabeu, C. Espinoza, C. Orme, S. Palomares-Ruiz and S. Pascoli, JHEP **0906** (2009) 040 [arXiv:0902.4903 [hep-ph]].

94. M. Rolinec and J. Sato, JHEP **0708**, 079 (2007) [arXiv:hep-ph/0612148].
95. J. N. Bahcall, Phys. Rev. **194**, 495 (1961).
96. C. Rubbia, arXiv:hep-ph/0609235.
97. A. Donini and E. Fernandez-Martinez, Phys. Lett. B **641**, 432 (2006) [arXiv:hep-ph/0603261].
98. D. Meloni, O. Mena, C. Orme, S. Palomares-Ruiz and S. Pascoli, JHEP **0807**, 115 (2008) [arXiv:0802.0255 [hep-ph]].
99. P. Huber and W. Winter, Phys. Rev. D **68**, 037301 (2003). A. Y. Smirnov, arXiv:hep-ph/0610198. H. Minakata, arXiv:0705.1009 [hep-ph].
100. A. M. Dziewonski and D. L. Anderson, Phys. Earth Planet. Interiors **25**, 297 (1981).
101. S. K. Agarwalla, S. Choubey, S. Goswami and A. Raychaudhuri, Phys. Rev. D **75** (2007) 097302 [arXiv:hep-ph/0611233]. S. K. Agarwalla, S. Choubey and A. Raychaudhuri, Nucl. Phys. B **771**, 1 (2007) [arXiv:hep-ph/0610333]. S. K. Agarwalla, S. Choubey and A. Raychaudhuri, Nucl. Phys. B **798**, 124 (2008) [arXiv:0711.1459 [hep-ph]].
102. See http://www.imsc.res.in/∼ino.
103. P. Coloma, A. Donini, E. Fernandez-Martinez and J. Lopez-Pavon, JHEP **0805**, 050 (2008) [arXiv:0712.0796 [hep-ph]].
104. S. K. Agarwalla, S. Choubey, A. Raychaudhuri and W. Winter, JHEP **0806** (2008) 090
105. S. Choubey, P. Coloma, A. Donini and E. Fernandez-Martinez, JHEP **0912**

(2009) 020 [arXiv:0907.2379 [hep-ph]]. [arXiv:0802.3621 [hep-ex]].

106. M. Mezzetto, Nucl. Phys. Proc. Suppl. **143** (2005) 309.

107. S. K. Agarwalla, S. Choubey and A. Raychaudhuri, Nucl. Phys. B **805** (2008) 305 [arXiv:0804.3007 [hep-ph]].

108. W. Winter, Phys. Rev. D **78** (2008) 037101 [arXiv:0804.4000 [hep-ph]].

109. C. Volpe, J. Phys. G **30** (2004) L1 [arXiv:hep-ph/0303222].

110. J. Serreau and C. Volpe, Phys. Rev. C **70** (2004) 055502 [arXiv:hep-ph/0403293].

111. G. C. McLaughlin, Phys. Rev. C **70** (2004) 045804 [arXiv:nucl-th/0404002].

112. C. Volpe, J. Phys. G **31** (2005) 903 [arXiv:hep-ph/0501233].

113. R. Lazauskas and C. Volpe, Nucl.Phys.A792:219-228,2007, [arXiv:0704.2724] .

114. G. C. McLaughlin and C. Volpe, Phys. Lett. B **591** (2004) 229 [arXiv:hep-ph/0312156].

115. A. B. Balantekin, J. H. de Jesus and C. Volpe, Phys. Lett. B **634** (2006) 180 [arXiv:hep-ph/0512310].

116. A. B. Balantekin, J. H. de Jesus, R. Lazauskas and C. Volpe, Phys. Rev. D **73** (2006) 073011 [arXiv:hep-ph/0603078].

117. N. Jachowicz and G. C. McLaughlin, Phys. Rev. Lett. **96** (2006) 172301 [arXiv:nucl-th/0604046].

118. C. Volpe, J. Phys. G **34** (2007) R1 [arXiv:hep-ph/0605033].

119. N. Jachowicz, G. C. McLaughlin and C. Volpe, arXiv:0804.0360 [nucl-th].

120. R. Lazauskas, A. B. Balantekin, J. H. De Jesus and C. Volpe, Phys. Rev. D **76** (2007) 053006 [arXiv:hep-ph/0703063].

121. P. S. Amanik and G. C. McLaughlin, Phys. Rev. C **75**, 065502 (2007)

[arXiv:hep-ph/0702207].

122. C. Volpe, N. Auerbach, G. Colo and N. Van Giai, Phys. Rev. C **65**, 044603 (2002) [arXiv:nucl-th/0103039].
123. A. G. Cocco, A. Ereditato, G. Fiorillo, G. Mangano and V. Pettorino, JCAP **0412** (2004) 002 [arXiv:hep-ph/0408031].
124. C. Volpe, J. Welzel, arXiv:0711.3237.
125. J. Engel, G. C. McLaughlin and C. Volpe, Phys. Rev. D **67** (2003) 013005 [arXiv:hep-ph/0209267].
126. A. B. Balantekin and G. M. Fuller, J. Phys. G **29**, 2513 (2003) [arXiv:astro-ph/0309519].
127. C. J. Horowitz, Phys. Rev. D **65**, 043001 (2002) [arXiv:astro-ph/0109209].
128. B. S. Meyer, G. C. McLaughlin and G. M. Fuller, Phys. Rev. C **58**, 3696 (1998) [arXiv:astro-ph/9809242].
129. M. Ruffert, H. T. Janka, K. Takahashi and G. Schaefer, Astron. Astrophys. **319** (1997) 122 [arXiv:astro-ph/9606181].
130. J. P. Kneller, G. C. McLaughlin and R. Surman, J. Phys. G **32**, 443 (2006) [arXiv:astro-ph/0410397].
131. P. Vogel and J. F. Beacom, Phys. Rev. D **60**, 053003 (1999) [arXiv:hep-ph/9903554].
132. J. F. Beacom, W. M. Farr and P. Vogel, Phys. Rev. D **66** (2002) 033001 [arXiv:hep-ph/0205220].
133. C. Volpe, Nucl. Phys. A **752** (2005) 38 [arXiv:hep-ph/0409357].
134. A. Bueno, M. C. Carmona, J. Lozano and S. Navas, Phys. Rev. D **74**, 033010 (2006).
135. J. Barranco, O. G. Miranda and T. I. Rashba, *Low energy neutrino exper-*

iments sensitivity to physics beyond the standard model, Phys. Rev. D **76**, 073008 (2007) [arXiv:hep-ph/0702175].

136. C. Volpe, Nucl. Phys. Proc. Suppl. **155** (2006) 97 [arXiv:hep-ph/0510242].
137. N. A. Smirnova and C. Volpe, Nucl. Phys. A **714** (2003) 441 [arXiv:nucl-th/0207078].
138. C. Volpe, Nucl. Phys. Proc. Suppl. **143** (2005) 43 [arXiv:hep-ph/0409249], and references therein.
139. S. K. Agarwalla and P. Huber, arXiv:0909.2257 [hep-ph].
140. S. K. Agarwalla, P. Huber and J. M. Link, arXiv:0907.3145 [hep-ph].
141. C. Ishihara, arXiv:0912.1002 [hep-ex].

Table 1: Best-fit values, 2σ, and 3σ intervals (1 dof) for the three flavor neutrino oscillation parameters from global data including solar, atmospheric, reactor and accelerator experiments (1).

parameter	best-fit	2σ	3σ
Δm^2_{21} $[10^{-5}\mathrm{eV}^2]$	$7.65^{+0.23}_{-0.20}$	7.25–8.11	7.05–8.34
$\lvert\Delta m^2_{31}\rvert$ $[10^{-3}\mathrm{eV}^2]$	$2.40^{+0.12}_{-0.11}$	2.18–2.64	2.07–2.75
$\sin^2\theta_{12}$	$0.304^{+0.022}_{-0.016}$	0.27–0.35	0.25–0.37
$\sin^2\theta_{23}$	$0.50^{+0.07}_{-0.06}$	0.39–0.63	0.36–0.67
$\sin^2\theta_{13}$	$0.01^{+0.016}_{-0.011}$	≤ 0.040	≤ 0.056

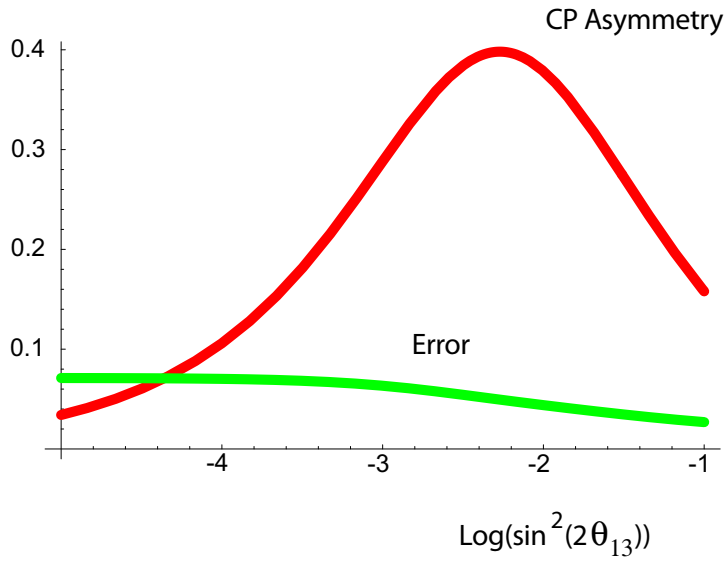

Figure 1: Magnitude of the CP asymmetry at the first oscillation maximum, for $\delta = 1$ as a function of the mixing angle $\sin^2 2\theta_{13}$. The curve marked "error" indicates the dependence of the statistical+systematic error on such a measurement. The curves have been computed for the baseline beta beam option at the fixed energy $E_\nu = 0.4$ GeV, $L = 130$ km, statistical + 2% systematic errors. From (31).

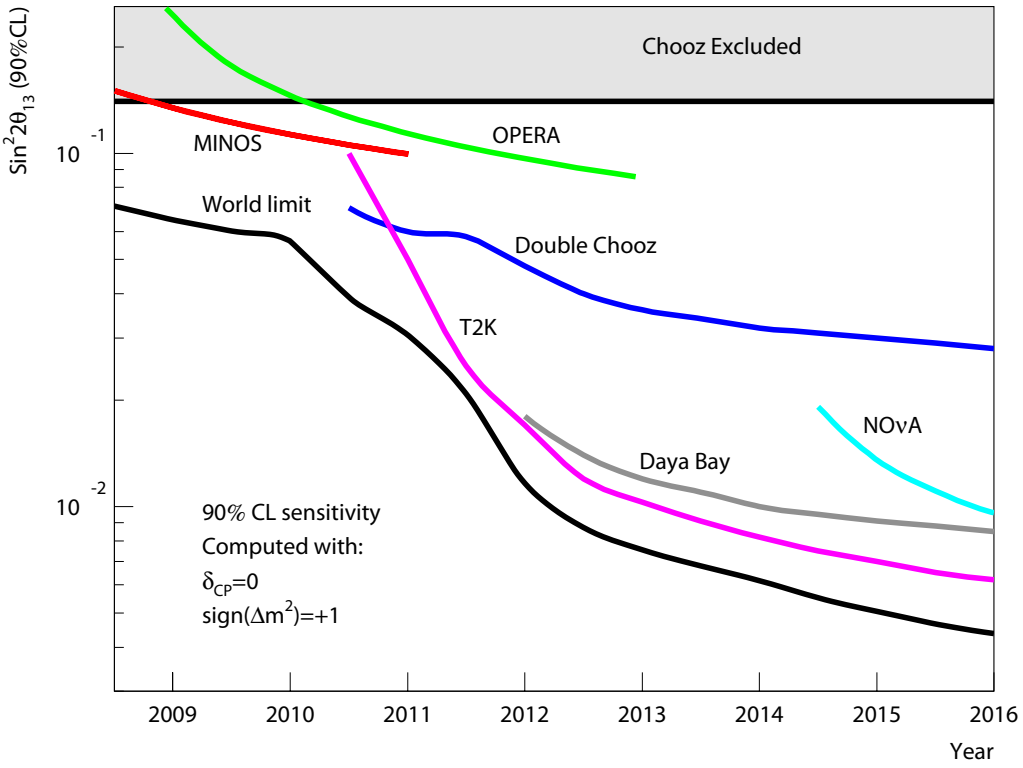

Figure 2: Evolution of experimental $\sin^2 2\theta_{13}$ sensitivities as function of time, computed assuming $\delta_{\rm CP} = 0$. Experiments are assumed to provide results after the first year of data taking, from (26)

.

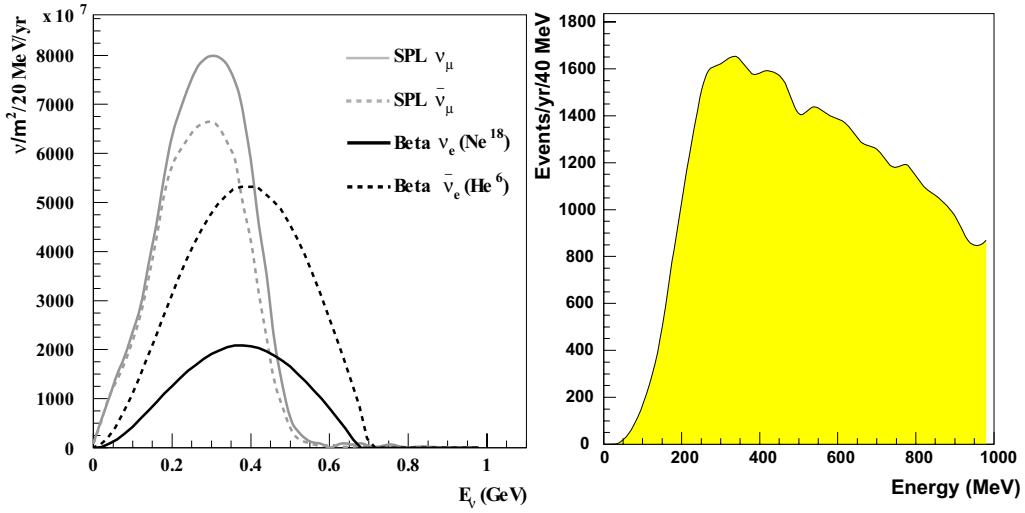

Figure 3: Left panel: neutrino flux of β-Beam ($\gamma = 100$) together with the CERN-SPL super beam, at 130 km of distance. Right panel: rate of atmospheric $\nu_\mu + \overline{\nu}_\mu$ interactions in MEMPHYS, integrated in one year.

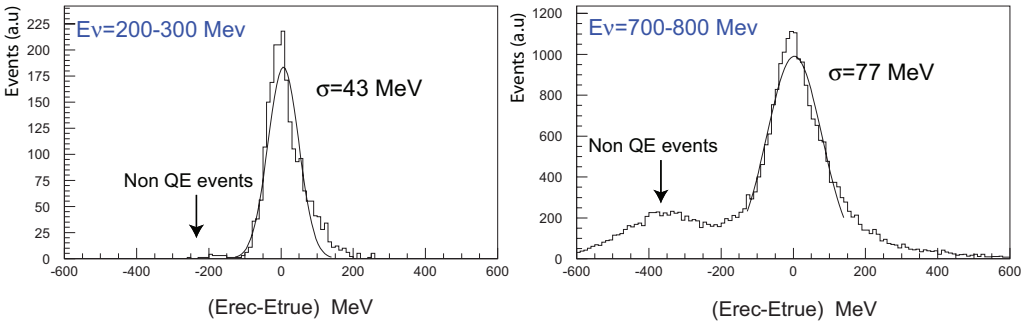

Figure 4: Energy resolution for ν_e interactions in the 200–300 MeV and 700–800 MeV energy ranges. The quantity displayed is the difference between the reconstructed and the true neutrino energy.

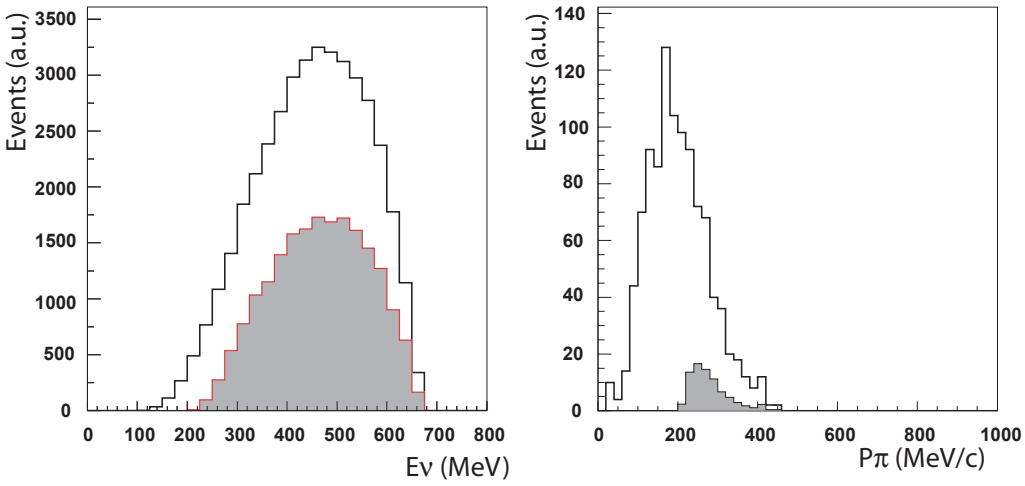

Figure 5: Left: Event reduction for ^{18}Ne oscillated events (left) and pion background, $\pi^+ + \pi^-$ (right).

Table 2: Summary of default parameters used for the simulation of the beta beam experiment.

Detector mass	440 kt
Baseline	130 km
Running time ($\nu + \bar{\nu}$)	5 + 5 yr
Beam intensity	$5.8\,(2.2) \cdot 10^{18}$ He (Ne) dcys/yr
Systematics on signal	2%
Systematics on backgr.	2%
Δm^2_{31}	$+2.4 \times 10^{-3}$ eV^2
$\sin^2\theta_{23}$	0.5
Δm^2_{21}	7.9×10^{-5} eV^2
$\sin^2\theta_{12}$	0.3

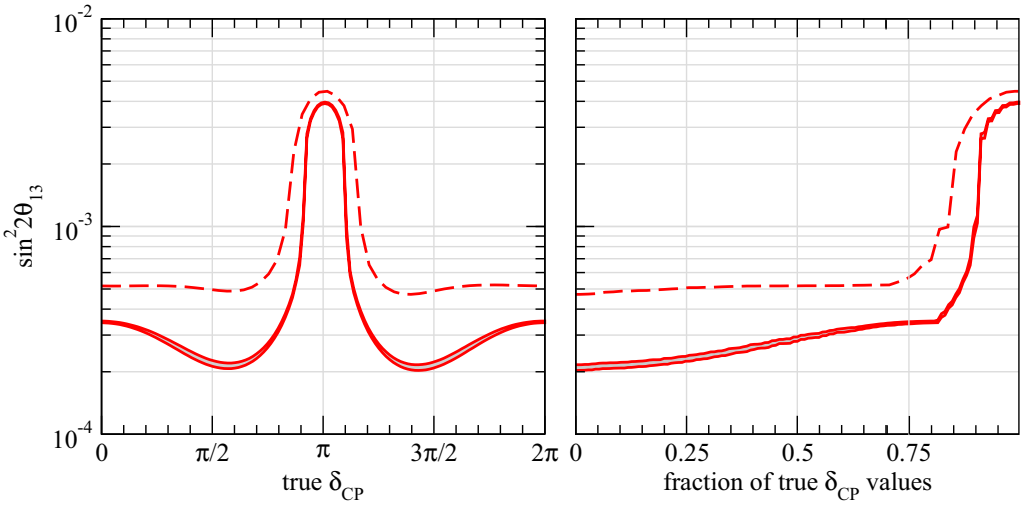

Figure 6: 3σ discovery sensitivity to $\sin^2 2\theta_{13}$ for beta beam, as a function of the true value of $\delta_{\rm CP}$ (left panel) and as a function of the fraction of all possible values of $\delta_{\rm CP}$ (right panel). The running time is $(5\nu + 5\bar{\nu})$ yrs. The width of the bands corresponds to values for systematical errors between 2% and 5%. The dashed curves show the sensitivity of the beta beam when the number of ion decays/yr is reduced by a factor of two with respect to the values given in Tab. 2.

Table 3: Characteristics of ^{8}B and ^{8}Li compared with ^{6}He and ^{18}Ne.

β^+ emitters			β^- emitters		
Ion	$Q_{\rm eff}$ (MeV)	Z/A	Ion	$Q_{\rm eff}$ (MeV)	Z/A
^{18}Ne	3.30	5/9	^{6}He	3.51	1/3
^{8}B	13.92	5/8	^{8}Li	12.96	3/8

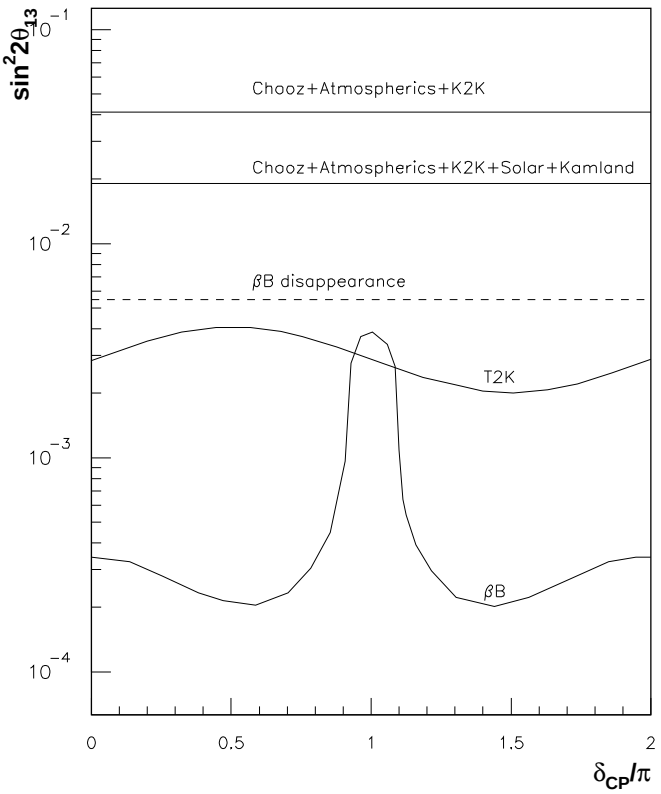

Figure 7: The same sensitivity curve as Fig. 6 (2% systematic errors), compared with the present world limits on θ_{13} (1) (solid lines), the 3σ T2K sensitivity computed for a 10 year neutrino run, and the CFBB sensitivity for the disappearance channel, computed for 1% systematic errors.

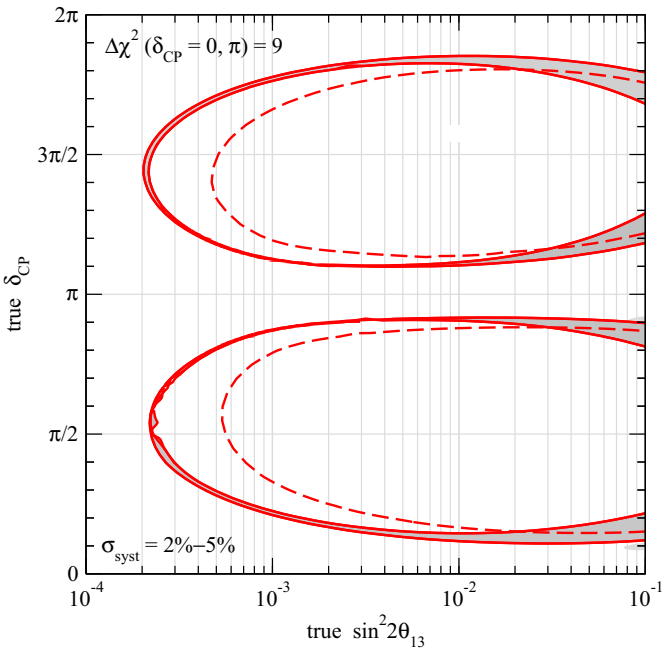

Figure 8: LCPV discovery potential: for parameter values inside the ellipse-shaped curves CP conserving values of $\delta_{\rm CP}$ can be excluded at 3σ ($\Delta\chi^2 > 9$). The running time is $(5\nu + 5\bar{\nu})$ yrs. The width of the bands corresponds to values for the systematical errors from 2% to 5%. The dashed curves show the sensitivity when the number of ion decays/yr are reduced by a factor of two with respect to the values given in Tab. 2 for 2% systematics.

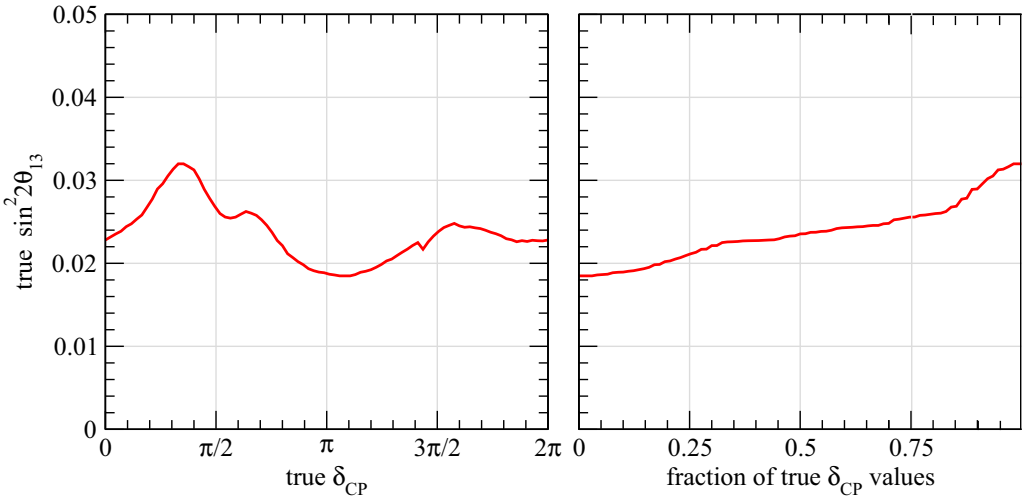

Figure 9: Sensitivity to the mass hierarchy at 2σ ($\Delta\chi^2 = 4$) as a function of the true values of $\sin^2 2\theta_{13}$ and $\delta_{\rm CP}$ (left), and the fraction of true values of $\delta_{\rm CP}$ (right). The solid curves are the sensitivities from the combination of long-baseline and atmospheric neutrino data, the dashed curves correspond to beta beam data only. The running time is $(5\nu + 5\bar{\nu})$ yrs.